Charging dynamics of a polymer due to electron irradiation: A simultaneous scattering-transport model and preliminary results*

Cao Meng(曹 猛), Wang Fang(王 芳), Liu Jing(刘 婧), and Zhang Hai-Bo(张海波)†

Key Laboratory for Physical Electronics and Devices of the Ministry of Education, Department of Electronic Science and Technology, Xi'an Jiaotong University, Xi'an 710049, *China*

(Received 27 April 2012; revised manuscript received 17 May 2012)

We present a novel numerical model and simulate preliminarily the charging process of a polymer subjected to electron irradiation of several 10 keV. The model includes the simultaneous processes of electron scattering and ambipolar transport and the influence of a self-consistent electric field on the scattering distribution of electrons. The dynamic spatial distribution of charges is obtained and validated by existing experimental data. Our simulations show that excess negative charges are concentrated near the edge of the electron range. However, the formed region of high charge density may extend to the surface and bottom of a kapton sample, due to the effects of the electric field on electron scattering and charge transport, respectively. Charge trapping is then demonstrated to significantly influence the charge motion. The charge distribution can be extended to the bottom as the trap density decreases. Charge accumulation is therefore balanced by the appearance and increase of leakage current. Accordingly, our model and numerical simulation provide a comprehensive insight into the charging dynamics of a polymer irradiated by electrons in the complex space environment.

Keywords: electron irradiation, charging dynamics, electron scattering, charge transport, polymer

PACS: 79.20.Ap, 72.20.Jv, 02.70.Uu **DOI:** 10.1088/1674-1056/21/12/127901

1. Introduction

Charging effects of dielectrics under electron irradiation have been extensively investigated since the spacecraft charging was reported by DeForest in 1972.[1] The irradiation in the outer space may lead to undesirable charging effects and disturb the smooth running of a spacecraft.[2−7] The anomaly diagnosis data indicate that the electrostatic discharge (ESD) from charging is an important cause of the formation of the anomalies of spacecrafts.[8] Here, the irradiation of several 10-keV electrons is mainly responsible for the serious internal charging in the ESD. On the other hand, polymeric materials are widely used in space technology. Therefore, to prevent or to get a better control over the initiation of ESD events, it is necessary to understand in more detail the irradiation-induced charging dynamics of a polymer under the irradiation of several 10-keV electrons.

The charging due to electron irradiation is a relatively complicated process including the simultaneous correlation with electron scattering and charge transport. Here, charge carriers consist of electrons and holes, and their transport should include both drift and diffusion. Moreover, the self-consistent electric field has effects not only on charge transport but also on electron scattering. The leakage current may also occur, which will of course affect the charging process, equilibrium, and strength. The pulsed electroacoustic technique, the pressure wave propagation, and other experimental methods have been developed to study the irradiation-induced charging effects.[9−11] However, it is difficult to directly measure the detailed information about the charging process, especially dynamic microscopic information about the motions of both electrons and holes. In the computational aspect, the widely used radiation-induced conductivity model adopts a macroscopic parameter to describe the interaction of incident electrons with the solid dielectric.[12−14] In this model, the ambipolar charge transport dynamics cannot be explicated. The generation–recombination model considers the generation of a carrier pair by incident electrons and the microscopic transport mechanisms of both elec-

*Project supported by the National Natural Science Foundation of China (Grant No. 11175140) and the Fundamental Research Funds for the Central Universities.

†Corresponding author. E-mail: hbzhang@mail.xjtu.edu.cn

© 2012 Chinese Physical Society and IOP Publishing Ltd

trons and holes.[15−18] The profile of carrier generation rate is conventionally obtained from measurements or Monte Carlo simulations.[19−21] This type of fixed profile cannot include the interaction between the self-consistent electric field and incident electrons in the dynamic charging process. In fact, variations of the self-consistent and external electric field can influence incident electrons, secondary electrons, and charge transport,[22−25] which may lead to a dynamic profile of the carrier generation rate. Therefore, a comprehensive model, which can consider electron scattering and charge transport simultaneously, is still desired for further investigation of the charging dynamics of a polymer due to electron irradiation. On the other hand, we have proposed a self-consistent model for charging effects of a grounded SiO_2 thin film due to a low-energy focused electron beam.[26]

To gain a distinct insight into the charging dynamics of an electron-irradiated polymer, in the present study we develop a comprehensive numerical model with simultaneous consideration of electron scattering and charge transport. Here, the scattering of incident electrons is simulated by the Monte Carlo method. The motions of charges are computed by considering diffusion, drift, trapping, and recombination. Some preliminary numerical results are presented on time evolutions of the internal charge distribution, surface potential, and leakage current.

2. Model and solution

2.1. Electron scattering

The electron–atom scattering as well as the ionization and electron deposition is simulated with the Monte Carlo method. Here, the scattering processes can be divided into two categories: elastic and inelastic scatterings. For an electron with energy higher than 10 keV, the elastic scattering process can be described by the screened relativistic Rutherford scattering cross section

$$\frac{\mathrm{d}\sigma(\theta)}{\mathrm{d}\Omega} = \frac{\lambda_{\mathrm{R}}^4 \bar{Z}^2}{64\pi^4 a_0^2 \Big[\sin^2\dfrac{\theta}{2} + \Big(\dfrac{\theta_0}{2}\Big)^2\Big]^2}. \tag{1}$$

Here, σ is the scattering cross section, θ the scattering angle, Ω the solid angle, λ_{R} the relativistic electron wavelength, $\bar{Z}$ the mean atomic number, a_0 the Bohr radius and θ_0 the screening factor.

The inelastic scattering process is described by the fast secondary electron model and the inelastic scattering cross section of the electron with an energy E is

$$\frac{\mathrm{d}\sigma}{\mathrm{d}\epsilon} = \frac{\pi e^4}{E^2}\Big[\frac{1}{\epsilon^2} + \frac{1}{(1-\epsilon)^2} + \Big(\frac{\tau}{1+\tau}\Big)^2 - \frac{2\tau+1}{(\tau+1)^2\epsilon(1-\epsilon)}\Big]. \tag{2}$$

Here ϵ denotes the energy transfer ΔE normalized with E; τ is the electron kinetic energy normalized by the rest mass energy of an electron, and e the elementary charge. Furthermore, the average energy loss rate is calculated by the modified Bethe equation of stopping power

$$\frac{\mathrm{d}E}{\mathrm{d}S} = -\frac{7.85\times10^4\rho\bar{Z}}{E\bar{A}}\ln\Big(\frac{1.166(E+k\bar{J})}{\bar{J}}\Big), \tag{3}$$

where S, $\bar{A}$, k, and $\bar{J}$ are the free path between two sequential scattering events, the mean atomic weight, the correction coefficient, and the mean ionization energy, respectively. In each inelastic scattering event, one secondary electron is generated after gaining the lost energy of the scattered primary electron. A hole is simultaneously generated at the scattering position. Both the scattered primary electron and the generated secondary electron will be further scattered and even produce more electrons and holes until the electrons exhaust their energies. Some electrons arriving at the sample surface may be emitted from the surface by overcoming the potential barrier at the surface. The distributions of electrons and holes induced by the incident electrons can then be obtained by the final states of the electrons and holes.

2.2. Charge transport

The electrons and the holes deposited in the polymer will drift and diffuse due to the internal self-consistent electric field and charge density gradient. Some charges may be trapped by trapping centres when transporting in the material. At the same time, electron–hole recombination will occur. In principle, the trapped charges may also be released again via detrapping. However, some experimental work shows that the charges in some polymers could persist for a long time,[12] which indicates that the detrapping effect is often very weak and therefore negligible.

The charging process is investigated by a model with a comprehensive consideration of scattering, drift, trapping, and recombination of charge carriers. The equations for free electron density n_{f}, trapped electron density n_{t}, and hole density p are given as

$$\frac{\partial n_{\mathrm{f}}}{\partial t} = \Big(\frac{\partial n_{\mathrm{f}}}{\partial t}\Big)_{\mathrm{scat}} + \Big(\frac{\partial n_{\mathrm{f}}}{\partial t}\Big)_{\mathrm{drift}} + \Big(\frac{\partial n_{\mathrm{f}}}{\partial t}\Big)_{\mathrm{dif}} + \Big(\frac{\partial n_{\mathrm{f}}}{\partial t}\Big)_{\mathrm{trap}} + \Big(\frac{\partial n_{\mathrm{f}}}{\partial t}\Big)_{\mathrm{rec}}, \tag{4}$$

$$\frac{\partial n_{\rm t}}{\partial t} = \Big(\frac{\partial n_{\rm t}}{\partial t}\Big)_{\rm trap} + \Big(\frac{\partial n_{\rm t}}{\partial t}\Big)_{\rm rec}, \tag{5}$$

$$\frac{\partial p}{\partial t} = \Big(\frac{\partial p}{\partial t}\Big)_{\rm scat} + \Big(\frac{\partial p}{\partial t}\Big)_{\rm drift} + \Big(\frac{\partial p}{\partial t}\Big)_{\rm dif} + \Big(\frac{\partial p}{\partial t}\Big)_{\rm rec}. \tag{6}$$

Here, we use subscripts scat, drift, dif, trap, and rec to represent the terms corresponding to scattering, drift, diffusion, trapping, and recombination, respectively. Note that hole trapping is ignored because it is negligible. Then, the term for scattering can be calculated from the charge distribution obtained by the Monte Carlo simulation. Here, the secondary electron emission and redistribution are considered together with the self-consistent electric field to give real-time information about their influences on electron scattering.

The terms for drifting and diffusing are treated using charge conservation equations as

$$\Big(\frac{\partial n}{\partial t}\Big)_{\rm drift} = \frac{1}{e}\boldsymbol{\nabla}\cdot\boldsymbol{J}^n_{\rm drift} = \boldsymbol{\nabla}\cdot\Big(\mu_n n\boldsymbol{E}\Big), \tag{7}$$

$$\Big(\frac{\partial n}{\partial t}\Big)_{\rm dif} = \frac{1}{e}\boldsymbol{\nabla}\cdot\boldsymbol{J}^n_{\rm dif} = \boldsymbol{\nabla}\cdot\Big(D_n\boldsymbol{\nabla}n\Big), \tag{8}$$

$$\Big(\frac{\partial p}{\partial t}\Big)_{\rm drift} = -\frac{1}{e}\boldsymbol{\nabla}\cdot\boldsymbol{J}^p_{\rm drift} = -\boldsymbol{\nabla}\cdot\Big(\mu_p p\boldsymbol{E}\Big), \tag{9}$$

$$\Big(\frac{\partial p}{\partial t}\Big)_{\rm dif} = -\frac{1}{e}\boldsymbol{\nabla}\cdot\boldsymbol{J}^p_{\rm dif} = \boldsymbol{\nabla}\cdot\Big(D_p\boldsymbol{\nabla}p\Big). \tag{10}$$

Here, superscripts n and p denote the parameters for electron and hole, respectively, $\boldsymbol{J}$ is the current density, $\boldsymbol{E}$ the electric field in the material, μ the carrier mobility, D the diffusion coefficient determined by the Nernst–Einstein equation, $D = \mu k_{\rm B}T/q$, with $k_{\rm B}$ being the Boltzmann constant. The electric field satisfies the Poisson's equation

$$\boldsymbol{\nabla}\cdot\boldsymbol{E} = -\frac{\rho}{\varepsilon}. \tag{11}$$

The carriers will leave the polymer via a leakage current if they arrive at the grounded substrate at the bottom.

A free electron is changed into a trapped one if it is trapped by a trapping centre. The trapping term can be denoted by

$$\Big(\frac{\partial n_{\rm f}}{\partial t}\Big)_{\rm trap} = -\frac{n_{\rm f}}{\tau_{\rm f}}\Big(1-\frac{n_{\rm t}}{N_{\rm T}}\Big), \tag{12}$$

where $\tau_{\rm f}$ is the lifetime of free electrons and $N_{\rm T}$ the trap density. Both free and trapped electrons may be recombined with the corresponding holes and the equations for recombination, respectively, are

$$\Big(\frac{\partial n_{\rm f}}{\partial t}\Big)_{\rm rec} = -\alpha_{\rm f} n_{\rm f} p, \tag{13}$$

$$\Big(\frac{\partial n_{\rm t}}{\partial t}\Big)_{\rm rec} = -\alpha_{\rm t} n_{\rm t} p. \tag{14}$$

Here $\alpha_{\rm f}$ and $\alpha_{\rm t}$ are the free and trapped electron–hole recombination rates, respectively

2.3. Numerical solution procedure

The time evolution of charges in the polymer can be investigated by solving Eqs. (4)–(6) numerically. For example, the solution procedure for the electron density is illustrated in Fig. 1. To discretize and numerically solve this problem, the sampling point sequence t_i is considered. At the initial time $t_0 = 0$, the values of $n_{\rm f}$ and $n_{\rm t}$ are set to be zero. For any sampling point t_i, the change rate of electron density $\partial n/\partial t$ is calculated by the method described in the above section. The value of n for t_{i+1} is obtained iteratively using

$$n(x,y,z,t_{i+1}) = n(x,y,z,t_i) + \Big(\frac{\partial n}{\partial t}\Big)_{t=t_i}(t_{i+1}-t_i). \tag{15}$$

Here, the time interval $t_{i+1} - t_i$ is adjusted according to the value of $\partial n/\partial t$. For a big value of $\partial n/\partial t$, a small time interval is chosen to reduce the numerical error. Otherwise, a big time interval is used to speed up computation. Computational skills given in Ref. [27] are used to enhance the numerical stability. The electric field and the surface potential are then updated according to the new charge distribution. The incident electron energy used in the next iteration step should be modified according to the surface potential. The simulation for the hole density can be performed similarly.

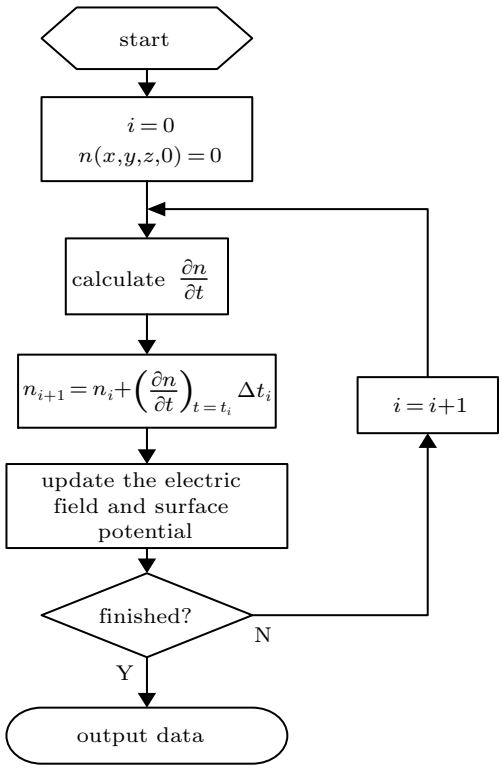


Fig. 1. Solution procedure of the electron density.

3. Results and discussion

3.1. Simulation condition

We use the above method to simulate charging characteristics of the grounded uniform polymer sample under a uniform electron irradiation shown in Fig. 2. The parameters for simulation are listed in Table 1. In principle, a complicated three-dimensional model is required to accurately describe a sample with an arbitrary structure. However, the one-dimensional model in this work can be seen as a prototype structure for a grounded polymer material in an electronic device. Therefore, our simulation results can still provide useful information about the polymer charging due to electron irradiation.

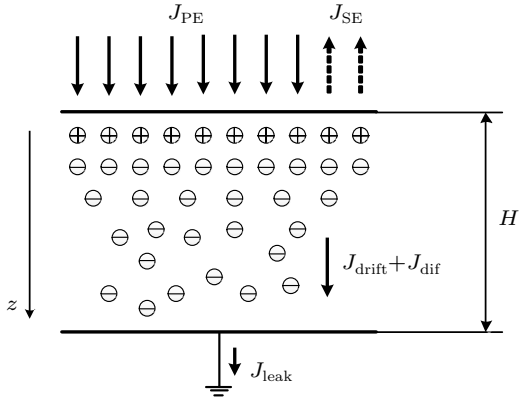


Fig. 2. Simulation configuration and currents in the process of uniform electron irradiation for a kapton sample. Here, $J_{\rm PE}$ and $J_{\rm SE}$ denote the current densities of incident and secondary electrons, respectively $J_{\rm leak}$ is the leakage current density from electrons, and current densities $J_{\rm drift}$ and $J_{\rm dif}$ are due to drift and diffusion in charge transport, respectively.

Table 1. Parameters of the kapton sample used in the simulation.

Parameter	Value
Relative dielectric constant ($\varepsilon_{\rm r}$)	3.4
Electron mobility ($\mu_{\rm n}$)	3.0×10^{-11} cm^2·V^{-1}·s^{-1}
Hole mobility ($\mu_{\rm p}$)	1.0×10^{-12} cm^2·V^{-1}·s^{-1}
Free electron–hole recombination rate ($\alpha_{\rm f}$)	1.6×10^{-16} cm^3·s^{-1}
Trapped electron–hole recombination rate ($\alpha_{\rm t}$)	1.6×10^{-16} cm^3·s^{-1}
Trap density ($N_{\rm T}$)	5.0×10^{16} cm^{-3}
Lifetime of free electrons ($\tau_{\rm f}$)	1 s
Sample thickness (H)	25 μm

3.2. Charging dynamics and charge evolution

The charges generated by electron scattering are the source for the irradiation-induced charging. Figure 3 shows the results of Monte Carlo simulation on the electron and hole change rates induced by scattering at different incident electron energies. We can see that the electron range formed by scattering increases with incident electron energy rising. This is in agreement with the continuous slowing down approximation range calculated by the ESTAR program,[28] validating our Monte Carlo simulation. On the other hand, the mean free path of inelastic scattering is much smaller than the electron range. Thus, hundreds of inelastic scattering events occur due to an incident electron so that many electron–hole pairs can be generated in the electron range. Consequently, the electrons and holes in the electron range are in a plasma state.

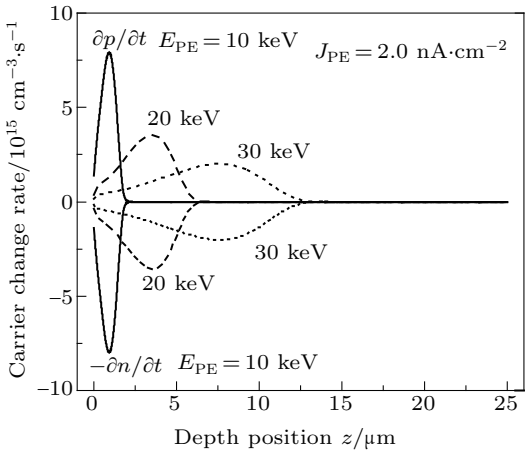


Fig. 3. Electron and hole change rates induced by scattering of incident electrons with different values of energy $E_{\rm PE}$ at a fixed current density $J_{\rm PE}$ in the simulation.

The properties of the charging process depend on irradiation time or total irradiation dose. We first look at the charge evolutions during and after irradiation. Here, the charge relaxation process is simulated by setting the incident electron current to be zero after the irradiation time $t = 20$ s. Figure 4 illustrates the quantities of total charges for free electrons, free holes, trapped electrons, and net charges on a unit area as functions of t. In the early stage of charging, both free electron and hole densities in the polymer are very low. The speed of trapping and recombination are much lower than the scattering. Therefore, the free electrons and holes both increase linearly with t when $t < 1$ s. The trapped electrons also increase linearly with t since the trapping is proportional to the free electron density. The increase in electron and hole densities is damped by the recombination and then tends to saturation in 3 s–5 s. The saturation of free electrons appears first since its increase is damped by both trapping and recombination. The increase in

trapped electron density also slows down due to the saturation of free electron density. The net charge density, however, keeps linearly increasing when the incident current is kept constant since little charge escapes from the surface. In the relaxation process, the densities of electrons and holes decrease exponentially due to the electron–hole recombination.

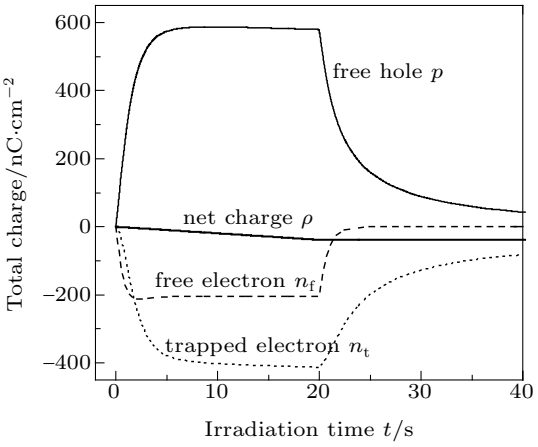


Fig. 4. Total charges for different kinds of charges versus irradiation time t during charging ($t < 20$ s) and relaxation process ($t > 20$ s).

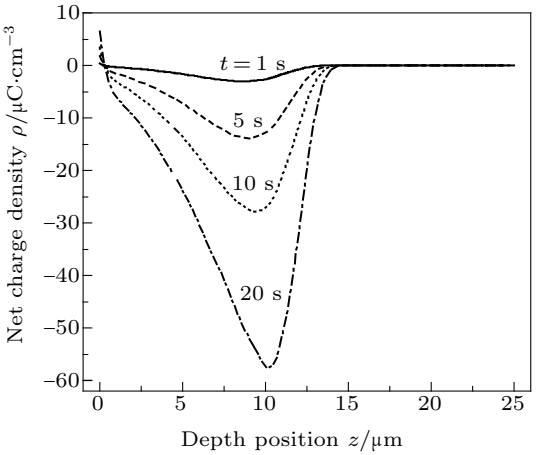


Fig. 5. Spatial distributions of net charges at different irradiation times.

The charge evolution can also be demonstrated by the charge distributions at different irradiation times. Figure 5 shows the net charge distributions at different irradiation times. For a small dose irradiation, the internal electric field is not strong and the charge transport is very slow. At the same time, most of the trapping centres are unoccupied. Therefore, most of the irradiation-induced charges are trapped or recombined at the generation position and the shape of the net charge distribution is close to that of the charge change rate shown in Fig. 3. The charges concentrate onto the bottom slightly by the electric force after $t = 10$ s. During the relaxation process after $t = 20$ s, there is little variation for the net charge distribution. The simulated steady state charge distribution is compared with the existing experimental data as shown in Fig. 6. A reasonable agreement is available here, though some deviations exist probably owing to the parameter difference between simulation and experiment or the accumulation effect of charges during the experiment.

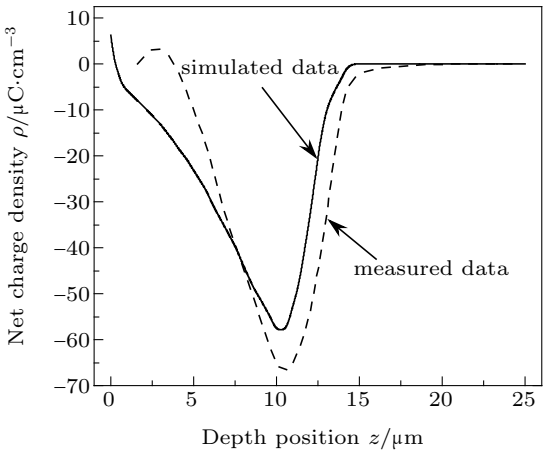


Fig. 6. Comparison of steady state charge distribution between the simulation results and the measured data in Ref. [12].

Under a short time irradiation, the distribution of the deposited charge changes slightly with the irradiation time because the internal electric field is weak. However, the charge distribution will be deformed by the electric field with the charge accumulation. We simulate its evolution during a long time irradiation till 800 s, in which the irradiation dose is chosen to make the internal electric field close to the breakdown level. Figure 7 shows the net charge distributions at different irradiation times. In Fig. 7(a), the net charge density is presented in a form of the gray scale map. The depth profiles of charges are illustrated at 20 s, 100 s, 200 s, and 800 s in Fig. 7(b). The full width at half maximum (FWHM) for a charge distribution is also plotted as a function of t in Fig. 7(c). The simulation results show the narrowing of the charge distribution when $t < 200$ s. With the charge accumulation in the electron range, the remaining unoccupied trapping centres tend to be exhausted and the excess negative charges drift toward the surface due to the self-consistent electric field. The value of the negative charge is also affected by the hole density. In the electron range, negative charges are balanced by the scattering-induced holes. The hole density is

much lower outside the electron range. Thus, the electrons concentrate near the edge of the electron range, forming a peak of the negative charge distribution.

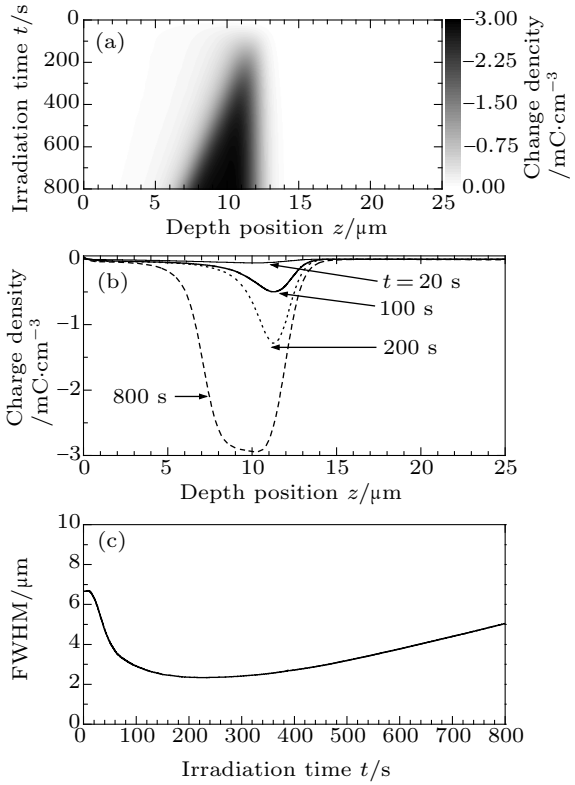


Fig. 7. (a) Gray scale map of time-dependent net charge profiles. (b) Net charge profiles at different irradiation times t. (c) FWHM for the charge distribution as a function of t.

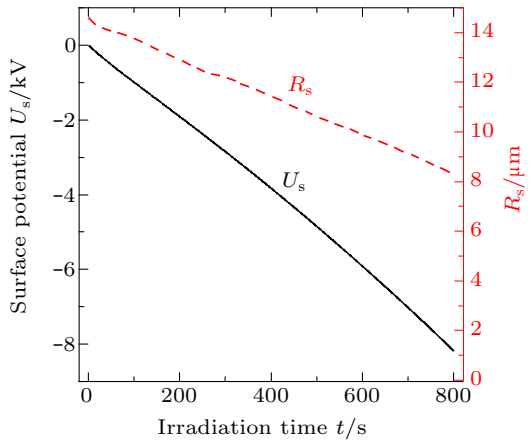


Fig. 8. (colour online) Surface potential U_s and electron range R_s each as a function of irradiation time.

The net charge distribution is broadened when $t > 200$ s, as shown in Figs. 7(b) and 7(c). This is due to the effect of the self-consistent electric field on incident electrons. With the negative charge accumulation, the self-consistent electric field forms a barrier at the surface. After overcoming the barrier, the landing energy of incident electron decreases. The electron range also decreases. Figure 8 further gives the surface potential U_s and the electron range R_s each as a function of t. At $t = 800$ s, the surface potential decreases to a value near -8 kV and the electron range decreases from 15 μm to 8 μm. Negative charges are thus deposited in a small depth region and the FWHM for the total net charge distribution becomes wider.

3.3. Charging equilibrium and leakage current

The leakage current is an important factor especially for the grounded polymer with a low trap density, because it directly affects the transient charging process and therefore the final equilibrium state of space charge distribution. Accordingly, we simulate the charge evolution under a long-period irradiation at which a steady state of charging will appear. In the simulation, the trap density is set to be 5×10^{15} cm^{-3} because a higher trap density could accumulate a large quantity of charges and cause the internal electric field beyond the breakdown level before equilibrium. Figure 9 illustrates the net charge distributions at different irradiation times. Here, charges accumulate first in the electron range. The accumulation in the range will be suspended by the recombination of trapped electrons and holes. Then, trapping will take place mainly outside the electron range, where trapping tends to saturation when all trapping centres have been occupied. The high charge density region extends toward the bottom after $t = 100$ s. At about $t = 600$ s, the high charge density region extends to the bottom. Figure 10 presents the total charge accumulated per unit area and the leakage current density each as a function of t. Before the high charge density region arrives at the bottom, the leakage current is very weak because of weak transport. Thus, the quantity of total charges per unit area increases linearly with irradiation time. However, the leakage current increases rapidly when the high charge density region has arrived at the grounded bottom. After a transient process, the leakage current trends to saturation. The saturation value of the leakage current density $J_{\rm leak}$ is equal to $J_{\rm PE} - J_{\rm SE}$ as illustrated in Fig. 2. Evidently, the currents flowing into and out of the sample are balanced and the net charge flux becomes zero. Consequently, the total charge quantity tends to its equilibrium state.

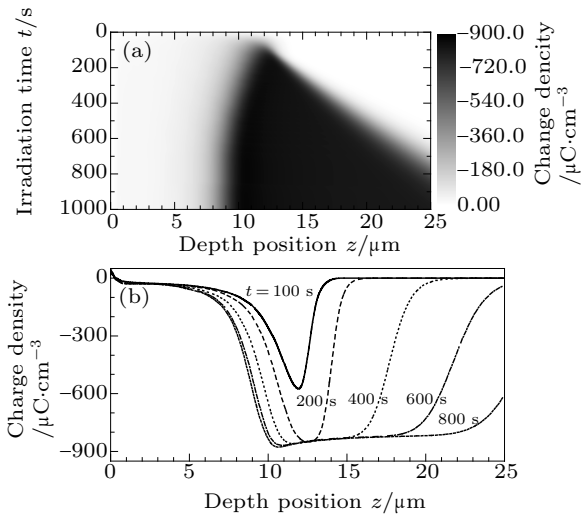


Fig. 9. (a) Gray scale map of time-dependent net charge profiles under a longtime irradiation. (b) Net charge profiles at different irradiation times.

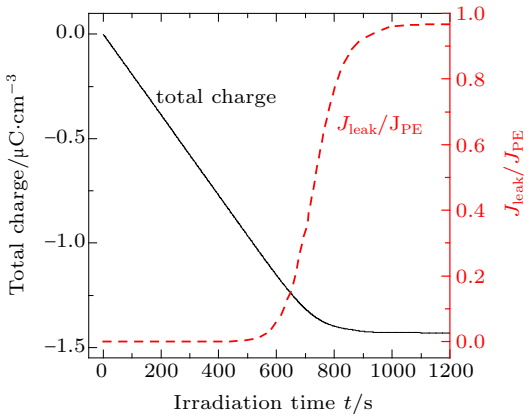


Fig. 10. (colour online) Total quantity of charges per unit area and the leakage current density J_{leak} with respect to the current density J_{PE} of incident electrons, each as a function of irradiation time.

4. Conclusions

We developed a new numerical model and simulated dynamic charging characteristics of a polymer subjected to electron irradiation. The simultaneous processes of electron scattering and charge transport are described accurately by including the effects of a self-consistent electric field. Here, the electric field could affect not only the charge transport beyond the electron range but also the distribution of high charge density. Preliminary simulation results show that the reduction of trap density could help prevent the charge accumulation because a lower trap density allows more charges to move toward the bottom, resulting in the leakage current and the saturation of charge accumulation. Further investigation can be suggested to quantify the effects of irradiation condition, polymer parameter, and sample structure on complicated charging processes of a polymer in the space environment.

Acknowledgement

The authors thank Wu Jun for assistance in modelling and simulation.

References

[1] DeForest S E 1972 *J. Geophys. Res.* **77** 651
[2] Lai S T and Tautz M 2008 *J. Geophys. Res.* **113** A11211
[3] Garrett H B, Evans R W, Whittlesey A C, Katz I and Jun I 2008 *IEEE Trans. Plasma Sci.* **36** 2440
[4] Rau E I, Evstafeva E N and Andrianov M V 2008 *Phys. Solid State* **50** 621
[5] Lai S T 2010 *J. Spacecraft Rockets* **47** 634
[6] Huang J G and Han J W 2010 *Acta Phys. Sin.* **59** 2907 (in Chinese)
[7] Kim W, Jun I and Kokorowski M 2010 *IEEE Trans. Nucl. Sci.* **57** 3143
[8] Koons H C, Mazur J E, Selesnick R S, Blake J B, Fennell J F, Roeder J L and Anderson P C 2000 *Proc. 6th Spacecraft Charging Technology Conference*, September 1–3, 2000, Bedford, MA, USA, p. 7
[9] Takada T, Miyake H and Tanaka Y 2006 *IEEE Trans. Plasma Sci.* **34** 2176
[10] Perrin C, Griseri V, Inguimbert C and Laurent C 2008 *J. Phys.* D: *Appl. Phys.* **41** 205417
[11] Zhao S L and Poumellec B 2011 *Chin. Phys.* B **20** 037901
[12] Sessler G M 1992 *IEEE Trans. Electr. Insul.* **27** 961
[13] Kotera M, Yamaguchi K and Suga H 1999 *Jpn. J. Appl. Phys.* **38** 7176
[14] Yasuda M, Kainuma Y, Kawata H, Hirai Y, Tanaka Y, Watanabe R and Kotera M 2008 *J. Appl. Phys.* **104** 124904
[15] Ferreira G F L and de Figueiredo M T 2003 *IEEE Trans. Dielectr. Electr. Insul.* **10** 137
[16] Touzin M, Goeuriot D, Guerret-Piecourt C, Juve D, Treheux D and Fitting H J 2006 *J. Appl. Phys.* **99** 114110
[17] Le Roy S, Baudoin F, Griseri V, Laurent C and Teyssedre G 2010 *J. Phys.* D: *Appl. Phys.* **43** 315402
[18] Quan R H, Zhang Z L, Han J W, Huang J G and Yan X J 2009 *Acta Phys. Sin.* **58** 1205 (in Chinese)
[19] Matsuoka S, Sunaga H, Tanaka R, Hagiwara M and Araki K 1976 *IEEE Trans. Nucl. Sci.* **23** 1447
[20] Berkley D A 1979 *J. Appl. Phys.* **50** 3447
[21] Qin X G, He D Y and Wang J 2009 *Acta Phys. Sin.* **58** 684 (in Chinese)
[22] Zhang H B, Feng R J and Ura K 2003 *Chin. Phys. Lett.* **20** 2011
[23] Cazaux J 2005 *J. Phys.* D: *Appl. Phys.* **38** 2433
[24] Zhang H B, Li W Q and Cao M 2012 *Chin. Phys. Lett.* **29** 047901
[25] Liu Z L, Hu Z Y, Zhang Z X, Shao H, Chen M, Bi D W, Ning B X and Zou S C 2011 *Chin. Phys.* B **20** 070701
[26] Li W Q and Zhang H B 2010 *Appl. Surf. Sci.* **256** 3482
[27] Le Roy S, Teyssedre G and Laurent C 2006 *IEEE Trans. Dielectr. Electr. Insul.* **13** 239
[28] http://physics.nist.gov/PhysRefData/Star/Text/ESTAR.html